An input saturation-tolerant position control method for magnetic microrobots using adaptive fuzzy sliding-mode method

Alireza Mousavi [+], Awais Ahmed [+], Hesam Khaksar, Hongsoo Choi, *Senior Member, IEEE*, and Ali Kafash Hoshiar, *Senior Member, IEEE*

***Abstract*—The position control of magnetic medical microrobots is influenced by several environmental uncertainties including the unknown characteristics of the medium and the imaging precision. Furthermore, measuring the physical attributes of the microrobots is a challenging issue. To provide a model-free position control approach for the magnetic medical microrobots, a saturation-tolerant Adaptive Fuzzy Sliding-Mode Control (AFSMC) is designed in this study. In the proposed approach, each control input comprises a fuzzy inference term utilized to approximate an unknown nonlinear function including uncertain forces, a robust part derived to compensate for the fuzzy approximation error and disturbances, and a compensating gain for input saturation. By utilizing the second theorem of Lyapunov and Barbalat's lemma, it is proved that the closed-loop system is asymptotically stable. The effectuality of the presented controller is assessed by means of two experimental scenarios. The results show that the magnitudes of the tracking errors corresponding to a spiral reference path are less than 0.2 mm at the end of the motion. Moreover, in the test conducted in a 3D printed Aorta phantom, the minimum and the maximum values of the tracking errors are -1.22 mm and 0.95 mm, respectively.**

***Note to Practitioners*—This article introduces an innovative, model-free technique specifically designed to tackle the complex challenges of position control in magnetic medical microrobots. Achieving precise control over these microrobots is a challenging task, compounded by the complexity of accurately measuring their physical properties and the characteristics of their surrounding medium. This challenge is further exacerbated by the issue of input saturation, which can compromise system stability. Our pioneering control method is designed to navigate these obstacles effectively. It functions under the assumption that both the lower and upper saturation limits are unknown, and it eliminates the necessity to model the forces acting on the microrobot. Experimental results confirm the method's effectiveness in accurately tracking various reference trajectories. These findings suggest that our method holds significant promise for various medical applications.**

***Index Terms*—Magnetic Manipulation, Microrobot, AFSMC, Motion Control.**

This work was financially supported by University of Essex Robotics and Embedded System research group and the National Convergence Research of Scientific Challenges through the National Research Foundation of Korea (NRF) (No. 2021M3F7A1082275) funded by the Ministry of Science and ICT. (Corresponding authors: Ali Kafash Hoshiar (a.kafashhoshiar@essex.ac.uk) and Hongsoo Choi (mems@dgist.ac.kr))

[+] Alireza Mousavi and Awais Ahmed have contributed equally to this work.

Alireza Mousavi, Hesam Khaksar, and Ali Kafash Hoshiar are with the School of Computer Science and Electronic Engineering, University of Essex, Colchester, CO4 3SQ, UK.

Awais Ahmed and Hongsoo Choi are with the Department of Robotics and Mechatronics Engineering and the DGIST-ETH Microrobotics Research Center, Daegu Gyeongbuk Institute of Science and Technology, Daegu 42988, South Korea.

I. Introduction

Over recent years, magnetically-actuated microrobots have been successfully employed in an extensive variety of medical applications including vascular interventions [1], [2], cancer treatment [3]–[5], hyperthermia therapy [6], targeted drug delivery [1], [7], [8], and microsurgery [1]. Magnetic actuation systems have emerged as the favored method of the microrobot manipulation due to safety, field generation dexterity, and precise control of the field [9].

In the practical applications, various architectures have been used to conduct the manipulation process. For instance, depending on the swimming mechanism, microrobots with helical [10]–[13], cylindrical [14], hexahedral or spherical [15] shapes have been employed. Moreover, magnetic resonance images [16], fluoroscopy method [17], and optical cameras [18] have been utilized for detection of the microrobot position.

In the motion control problem of the magnetic microrobots, it is difficult to measure the physical attributes of the microrobot and its surrounding medium. Accordingly, the lift force, the drag force, the weight, and the buoyant force are assumed to be unknown. It should be mentioned that, due to the complexities of modeling, the electrostatic force, the van der Waals force, the contact force at the fluid container surface, and the inertial force resulting from the added-mass effect cannot be derived [19]. Furthermore, the imaging noise in the detection of the position can result in performance degradation of the controller.

In previous studies, numerous attempts have been made to develop appropriate control methods for the manipulation of the microrobots. As reported in [20], the PID method with constant gains was unable to maintain a high level of tracking performance in control of the microrobot position when some changes were made in the system physical properties. To improve the control performance, some control structures have been proposed for the manipulation of the microrobots based on the adaptive PID method [20], the H-infinity control [21], the recursive least square method [18], the optimal control [22], [23], and the adaptive backstepping technique [24]. However, the control schemes proposed in [21], [22], [24] require model information. Furthermore, in [18], [20], [23], [24], only the 2-DOF motion of the microrobot has been considered in the design of the control structure. In [25], a control policy was developed for microrobotic systems using the broad learning

system (BLS) and employed to control a miniature helical swimmer. However, the process of designing and training the BLS-based controller is a constrained optimization problem. Furthermore, in [26], a strategy was proposed for completely decoupled independent control of a group of magnetically actuated flexible millirobots. Hence, the control objective in [26] is different from that of the above-mentioned studies.

In [27], the time-delay control (TDC) method as a robust control law was introduced for controlling the 3-DOF motion of the magnetic microrobots. The TDC method uses the previous time-step information of the system to estimate the current values of the control inputs. According to the results reported in [27], the TDC has reduced the steady-state error, the convergence time, and the magnitude of the overshoot in comparison to the methods mentioned above. In continuation, to avoid the windup phenomenon, a TDC-based structure has been designed in [19] including an anti-windup scheme. To put the TDC-based methods into practice, it is not needed to employ precise model information. However, a matrix containing the nominal value of the microrobot mass must be used which is difficult to determine. As it has been investigated in [28], the performance of the TDC-based methods is affected by the nominal mass matrix set by the user. Furthermore, in the anti-windup-based TDC approach, several tuning parameters should be chosen on the basis of the Lyapunov stability method. In consequence, the users of the magnetic microrobots experience some hardships in the tuning stage of the anti-windup-based TDC.

In this research, to deal with the limitations of the TDC-based methods, a model-free position control structure is designed for the magnetic medical microrobots based on the idea of adaptive fuzzy sliding-mode control (AFSMC). To control nonlinear systems with unknown dynamics, indirect and direct structures of AFSMC have been introduced. In the indirect AFSMC, the SMC model-based term is replaced by a fuzzy approximator. Furthermore, the upper bound of the uncertainty and the output vector of the fuzzy approximator are computed by the designed adaptation laws. While in the direct AFSMC which is more effective than the indirect approach [29], each control input includes an adaptively-tuned fuzzy approximator for an unknown function containing the system dynamics and an adaptive robust compensator for the fuzzy approximation error and uncertainties. Contrary to the anti-windup-based TDC approach, the tuning parameters of the direct AFSMC are selected without prior knowledge about the dynamic system. Moreover, the users do not need to use the nominal mass matrix in the design of the direct AFSMC.

Up to now, the direct AFSMC has been developed for under-actuated systems [30], multiple-input multiple-output systems in which the gain of the input vector is a non-diagonal and non-positive definite square matrix [29], [31], and non-square systems [32]. Moreover, the idea of saturation compensating gains has been employed to guarantee the stability of the direct AFSMC in the existence of input saturation [33]. However, the controller presented in [33] has been designed for single-input single-output nonlinear systems and cannot be utilized for the control of the magnetic microrobots which are moved by means of some electromagnetic coils.

In [28], the direct AFSMC has been employed for the position control problem of magnetic microrobots. The simulation results reported in [28] reveal the superiority of the direct AFSMC over the anti-windup-based TDC method. However, in the design of the AFSMC for the considered application, the compensation of the actuator saturation has not been addressed. It should be pointed out that the saturation of control inputs can lead to instability of the microrobots. Hence, to avoid performance deterioration and physical damage to the body of the patient in the presence of the input saturation, it is of high importance to redesign the direct AFSMC based on the idea of saturation compensating gains for controlling the magnetic microrobots.

In this study, to control the position of the magnetic microrobots, a saturation-tolerant direct AFSMC method is proposed. In the presented method, each adaptive fuzzy sliding-mode control input consists of a fuzzy inference system, a robust part, and a compensating gain for input saturation. The fuzzy inference system is utilized to approximate an unknown nonlinear function which includes uncertain forces and the robust part of the controller is considered to compensate for the fuzzy approximation error and disturbances. In addition, the compensating gain is designed to guarantee the asymptotic stability when the input saturation occurs. It is worth noting that, the adaptation laws of the control structure are derived with the help of the second theorem of Lyapunov.

The closed-loop structure for the position control of the magnetic microrobot is presented in Fig. 1. In this structure, the sampling rate of the controller should be determined based on the compuational complexity of the proposed AFSMC and the framerate of the cameras as the position sensors of the microrobot. Since the performance of the AFSMC in tracking tasks can be influenced by the choice of sampling rate, the effectuality of the proposed controller is evaluated through experimental tests.

The organization of the article is as follows: In Section II, the dynamic behavior of the system is modeled and the control

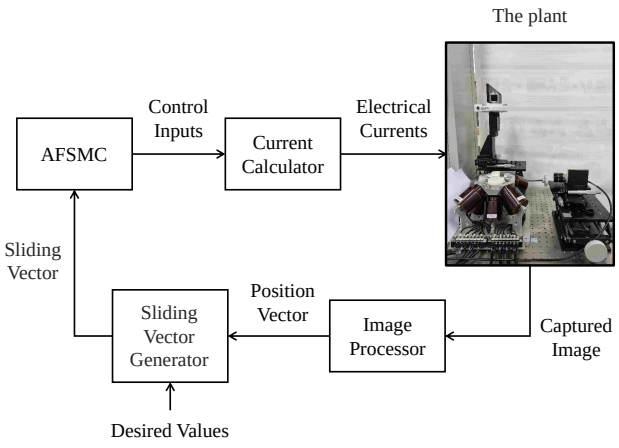

Figure 1: The closed-loop structure designed for the position control of the magnetically-actuated microrobot

objective is defined. In Section III, the design procedure of the saturation-tolerant AFSMC as well as the asymptotic stability analysis are presented. In Section IV, the results of the experimental tests are reported. Finally, conclusions and suggestions for future works are given in Section V.

II. Problem Definition

In this problem, by introducing the position vector of the microrobot $\mathbf{X} = [x, y, z]^{\mathrm{T}}$ and the mass m, the equation of motion by considering 3 degrees of freedom is obtained as

$$\ddot{\mathbf{X}} = \frac{1}{m}\left[\mathrm{sat}(\mathbf{F}_m) + \mathbf{F}_\Delta + \mathbf{F}_{\mathrm{tot}}\right]. \tag{1}$$

Here, $\mathbf{F}_m = [F_{m1}, F_{m2}, F_{m3}]^{\mathrm{T}}$ denotes the magnetic force vector as the control input, $\mathbf{F}_\Delta$ is the uncertain term of the magnetic force defined in the following, and $\mathbf{F}_{\mathrm{tot}}$ is the sum of all external forces acting on the microrobot, such as the weight, the buoyant force, the lift force, and the drag force. Due to the limitations of the actuation system in generating the magnetic forces, the saturation in control inputs has to be considered in modeling of the dynamic system. Hence, the saturated input vector $\mathrm{sat}(\mathbf{F}_m) = [\mathrm{sat}(F_{m1}), \mathrm{sat}(F_{m2}), \mathrm{sat}(F_{m3})]^{\mathrm{T}}$ is defined based on

$$\mathrm{sat}(F_{mi}) = \begin{cases} F_{m,\max}, & F_{mi} \geq F_{m,\max} \\ F_{mi}, & F_{m,\min} \leq F_{mi} \leq F_{m,\max} \\ F_{m,\min}, & F_{mi} \leq F_{m,\min} \end{cases} \quad (i = 1, 2, 3) \tag{2}$$

where $F_{m,\min} < 0$ and $F_{m,\max} > 0$ are the symbols of the lower and the upper saturation limits, respectively.

In the employed actuation system, the magnetic force vector $\mathbf{F}_m$ is generated as

$$\mathbf{F}_m = (\mathbf{M}.\nabla)\mathbf{B} \tag{3}$$

where $\mathbf{B} \in \mathbb{R}^{(3\times1)}$ is the magnetic field which is generated by the electromagnets, ∇ is the gradient operator, and $\mathbf{M} \in \mathbb{R}^{(3\times1)}$ is the magnetic moment [19]. If the vector $\mathbf{B}$ does not rotate too rapidly, we can assume that the microrobot and the vector $\mathbf{B}$ are always aligned. The validity of this assumption has been explored in [34]. Thus, by introducing $\hat{\mathbf{u}}_{\mathbf{B}}$ as the direction vector of $\mathbf{B}$, we have

$$\hat{\mathbf{u}}_{\mathbf{B}} = \frac{\mathbf{B}}{||\mathbf{B}||} = \frac{\mathbf{M}}{||\mathbf{M}||} \tag{4}$$

and equation (3) is rewritten as

$$\mathbf{F}_m = ||\mathbf{M}|| \begin{bmatrix} \frac{\partial \mathbf{B}}{\partial x} \\ \frac{\partial \mathbf{B}}{\partial y} \\ \frac{\partial \mathbf{B}}{\partial z} \end{bmatrix} \hat{\mathbf{u}}_{\mathbf{B}} = \begin{bmatrix} \frac{\partial \mathbf{B}}{\partial x} \\ \frac{\partial \mathbf{B}}{\partial y} \\ \frac{\partial \mathbf{B}}{\partial z} \end{bmatrix} \mathbf{M}. \tag{5}$$

In this problem, it is assumed that the magnetic field vector $\mathbf{B}$ is obtained by the linear superposition of the magnetic fields generated by the electromagnetic coils [35]. Using the linear superposition method for computing the vector $\mathbf{B}$ is valid under the following ideal circumstances: the cores are utilized in the linear magnetization regions and the material hysteresis of the soft magnetic cores is negligible [19]. Each coil generates a magnetic field proportional to its corresponding electrical current. Therefore, by defining $\mathbf{I}$ as the vector of currents flowing through the coils and the matrix of coefficients $\mathbf{K}$, the relationship between the magnetic force vector $\mathbf{F}_m$ and the vector $\mathbf{I}$ is presented as

$$\mathbf{F}_m = \mathbf{K}(\mathbf{X}, \mathbf{M})\mathbf{I}. \tag{6}$$

In order to compute the required vector $\mathbf{I}$ using (6), the matrix $\mathbf{K}$ should be determined. Ideally, a calibrated model is derived for the coefficient matrix $\mathbf{K}$ to map the magnetic field $\mathbf{B}$ and gradient field at any point in the workspace of the microrobot [35]. Since it can be assumed that the region surrounding the center is uniform in nature, in our case we use a constant matrix $\mathbf{K}$ at the center of the workspace. It should be noted that, the uniformity in the matrix $\mathbf{K}$ decreases as we move outwards from the center point. Since equation (4) as an assumption is not perfectly valid and the coils are assumed to be ideal, it is necessary to consider the uncertainty force $\mathbf{F}_\Delta$ in the dynamic equation (1).

In this study, we aim to design a direct AFSMC for the position control of the microrobot. Accordingly, the control objective should be presented based on the definition of sliding variables. By introducing the desired position vector $\mathbf{X}_d = [x_d, y_d, z_d]^{\mathrm{T}}$, the error vector $\tilde{\mathbf{X}} = [\tilde{x}, \tilde{y}, \tilde{z}]^{\mathrm{T}}$ is defined as

$$\tilde{\mathbf{X}} = \mathbf{X}_d - \mathbf{X}. \tag{7}$$

According to (7), the vector of sliding variables is generated in the form of

$$\mathbf{s} = [s_1, s_2, s_3]^{\mathrm{T}} = \dot{\tilde{\mathbf{X}}} + \boldsymbol{\lambda}\tilde{\mathbf{X}} \tag{8}$$

where $\boldsymbol{\lambda} = \mathrm{diag}(\lambda_1, \lambda_2, \lambda_3)$ is a positive definite diagonal matrix. Hence, the first-order representation of the dynamic system (1) is obtained as

$$\dot{\mathbf{s}} = \ddot{\mathbf{X}}_d - \frac{1}{m}\left[\mathrm{sat}(\mathbf{F}_m) + \mathbf{F}_\Delta + \mathbf{F}_{\mathrm{tot}}\right] + \boldsymbol{\lambda}\dot{\tilde{\mathbf{X}}}. \tag{9}$$

Based on the above-mentioned notes, the control objective is defined as follows:

Problem 1. Find the magnetic force $\mathbf{F}_m$ such that the asymptotic stability of the sliding variables is reached as $\lim_{t\to\infty} \mathbf{s} = 0$ subject to the dynamic system (1).

III. Saturation-tolerant AFSMC

A. Design of the adaptive control structure

In this study, the AFSMC is designed with the help of the positive definite function $V_1(\mathbf{s})$ which is proposed as

$$V_1(\mathbf{s}) = \frac{m}{2}\mathbf{s}^{\mathrm{T}}\mathbf{s}. \tag{10}$$

Hence, the time derivative of $V_1(\mathbf{s})$ is obtained as

$$\dot{V}_1 = m\mathbf{s}^{\mathrm{T}}\dot{\mathbf{s}}. \tag{11}$$

Furthermore, $\mathrm{sat}(\mathbf{F}_m)$ is rewritten as

$$\mathrm{sat}(\mathbf{F}_m) = \Theta \times \mathbf{F}_m \tag{12}$$

where the normalized saturation matrix $\Theta = \mathrm{diag}(\theta_1, \theta_2, \theta_3)$ is defined based on

$$\theta_i = \begin{cases} \dfrac{F_{m,\max}}{F_{mi}}, & F_{mi} \geq F_{m,\max} \\ 1, & F_{m,\min} \leq F_{mi} \leq F_{m,\max} \\ \dfrac{F_{m,\min}}{F_{mi}}, & F_{mi} \leq F_{m,\min} \end{cases} \quad (i = 1, 2, 3). \tag{13}$$

By proposing the vector $\boldsymbol{\beta}^* = [\beta_1^*, \beta_2^*, \beta_3^*]^{\mathrm{T}}$ in the form of

$$\boldsymbol{\beta}^* = m\ddot{\mathbf{X}}_d - (\mathbf{F}_\Delta + \mathbf{F}_{\mathrm{tot}}) + m\boldsymbol{\lambda}\dot{\tilde{\mathbf{X}}} \tag{14}$$

and using (9) and (11), we have

$$\dot{V}_1 = \mathbf{s}^{\mathrm{T}}(m\dot{\mathbf{s}}) = \mathbf{s}^{\mathrm{T}}(\boldsymbol{\beta}^* - \Theta \times \mathbf{F}_m). \tag{15}$$

The stability condition of the dynamic system (1) is considered as $\dot{V}_1 \leq 0$. Consequently, to achieve the control objective according to Problem 1, the input vector $\mathbf{F}_m$ should be designed based on the vector $\boldsymbol{\beta}^*$ and the matrix Θ which are assumed to be unknown. It should be noted that, according to (13), a positive constant ϑ_i exists such that $0 < \vartheta_i \leq \theta_i \leq 1$.

To design the AFSMC, since the components of the vector $\boldsymbol{\beta}^*$ are unknown, 3 fuzzy systems are proposed as the approximators of β_i^* $(i = 1, 2, 3)$. Because β_i^* is a function of the state variables of the i-th subsystem, s_i is considered as the input of the i-th fuzzy approximator. To construct the i-th fuzzy system, the rules of inference are suggested as follows.

$$\text{Rule } r\text{: If } s_i = A_i^r, \text{ then } \beta_i^{\mathrm{fuz}} = b_i^r.$$

Here, $r = 1, \ldots, 5$, A_i^r represents a fuzzy set, and b_i^r denotes the output value for the r-th rule of the i-th fuzzy approximator. In this research, the linguistic terms "Big Negative" $(r = 1)$, "Negative" $(r = 2)$, "Zero" $(r = 3)$, "Positive" $(r = 4)$, and "Big Positive" $(r = 5)$ are defined for the sliding variable s_i. For $r = 2, 3, 4$, the membership functions of the fuzzy sets A_i^r are constructed in the form of Gaussian functions as

$$\mu_{A_i^r}(s_i) = \exp\left[-\frac{(s_i - c_i^r)^2}{2{\sigma_i^r}^2}\right] \tag{16}$$

with shape parameters c_i^r and σ_i^r. Moreover, for $r = 1$ and $r = 5$, the sigmoidal membership functions are defined as

$$\mu_{A_i^r}(s_i) = \frac{1}{1 + \exp\left[-\frac{(s_i - c_i^r)}{\sigma_i^r}\right]}. \tag{17}$$

To partition the input domain of the sets A_i^r in a meaningful manner, the components of $\mathbf{c}_i = \left[c_i^1, c_i^2, c_i^3, c_i^4, c_i^5\right]^{\mathrm{T}}$ and $\boldsymbol{\sigma}_i = \left[\sigma_i^1, \sigma_i^2, \sigma_i^3, \sigma_i^4, \sigma_i^5\right]^{\mathrm{T}}$ are selected arbitrarily by user.

For constructing the approximators, the singleton fuzzification, the product inference, and the center average defuzzification methods are utilized. Hence, by defining the function

$$w_i^r = \frac{\mu_{A_i^r}(s_i)}{\sum_{r=1}^{5} \mu_{A_i^r}(s_i)}, \tag{18}$$

the output of the i-th fuzzy approximator is obtained as

$$\beta_i^{\mathrm{fuz}} = \mathbf{b}_i^{\mathrm{T}} \mathbf{w}_i \tag{19}$$

where $\mathbf{b}_i = \left[b_i^1, \ldots, b_i^5\right]^{\mathrm{T}}$ and $\mathbf{w}_i = \left[w_i^1, \ldots, w_i^5\right]^{\mathrm{T}}$. The structure of the fuzzy system designed for approximating β_i^* $(i = 1, 2, 3)$ is shown in Fig. 2.

By introducing $\mathcal{W}_i$ and $\mathcal{S}_i$ as the compact sets of $\mathbf{b}_i$ and s_i, the ideal output vector and the minimum approximation error corresponding to the i-th fuzzy system are defined in the form of

$$\mathbf{b}_i^* = \mathrm{argmin}_{\mathbf{b}_i \in \mathcal{W}_i} \left[\sup_{s_i \in \mathcal{S}_i} |\mathbf{b}_i^{\mathrm{T}} \mathbf{w}_i - \beta_i^*|\right] \tag{20}$$

and

$$\psi_i = \beta_i^* - {\mathbf{b}_i^*}^{\mathrm{T}} \mathbf{w}_i, \tag{21}$$

respectively. It should be noted that, according to the general approximation properties of the fuzzy systems [36], ψ_i is assumed to be bounded as

$$|\psi_i| < \Psi_i \tag{22}$$

where Ψ_i is an unknown positive value.

In this paper, the AFSMC input F_{mi} $(i = 1, 2, 3)$ is proposed as

$$F_{mi} = \hat{\gamma}_i \left(\hat{\beta}_i^{\mathrm{fuz}} + u_i^{\mathrm{rb}}\right) \tag{23}$$

where $\hat{\beta}_i^{\mathrm{fuz}}$ as the fuzzy part of the controller is generated as

$$\hat{\beta}_i^{\mathrm{fuz}} = \hat{\mathbf{b}}_i^{\mathrm{T}} \mathbf{w}_i, \tag{24}$$

the robust compensator u_i^{rb} is computed as

$$u_i^{\mathrm{rb}} = \left(\hat{\Psi}_i + 2\left|\hat{\mathbf{b}}_i^{\mathrm{T}} \mathbf{w}_i\right|\right) \mathrm{sgn}(s_i), \tag{25}$$

and $\hat{\gamma}_i$ is the saturation compensating gain. Furthermore, $\hat{\mathbf{b}}_i$, $\hat{\Psi}_i$, and $\hat{\gamma}_i$ respectively represent the approximate values of $\mathbf{b}_i^*$, Ψ_i, and ϑ_i^{-1}.

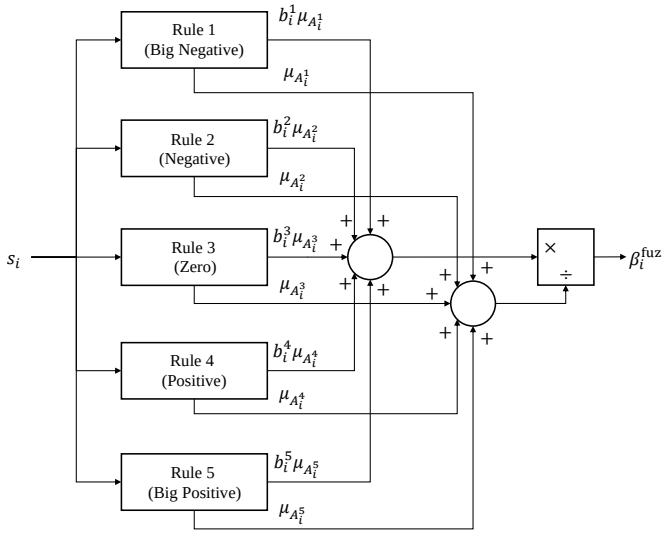

Figure 2: The structure of the fuzzy system designed for approximating β_i^* $(i = 1, 2, 3)$

To compute the values of $\hat{\mathbf{b}}_i$, $\hat{\Psi}_i$, and $\hat{\gamma}_i$, the adaptation laws of the AFSMC are proposed as

$$\dot{\hat{\mathbf{b}}}_i = \alpha_{1i} s_i \mathbf{w}_i, \tag{26}$$

$$\dot{\hat{\Psi}}_i = \alpha_{2i} |s_i|, \tag{27}$$

and

$$\dot{\hat{\gamma}}_i = \alpha_{3i} \hat{\gamma}_i^3 \left(|s_i| \hat{\Psi}_i + \left| s_i \hat{\mathbf{b}}_i^{\mathrm{T}} \mathbf{w}_i \right| \right). \tag{28}$$

Here, α_{1i}, α_{2i}, and α_{3i} $(i = 1, 2, 3)$ are arbitrary positive parameters determining the rates of learning in the AFSMC. Moreover, the initial conditions of $\hat{\Psi}_i$ and $\hat{\gamma}_i$ must be positive.

By defining $\hat{\boldsymbol{\gamma}} = \mathrm{diag}(\hat{\gamma}_1, \hat{\gamma}_2, \hat{\gamma}_3)$, $\hat{\boldsymbol{\beta}}^{\mathrm{fuz}} = \left[\hat{\beta}_1^{\mathrm{fuz}}, \hat{\beta}_2^{\mathrm{fuz}}, \hat{\beta}_3^{\mathrm{fuz}}\right]^{\mathrm{T}}$, and $\mathbf{u}^{\mathrm{rb}} = \left[u_1^{\mathrm{rb}}, u_2^{\mathrm{rb}}, u_3^{\mathrm{rb}}\right]^{\mathrm{T}}$ and using (23), the vector of AFSMC inputs is obtained as

$$\mathbf{F}_m = \hat{\boldsymbol{\gamma}} \left(\hat{\boldsymbol{\beta}}^{\mathrm{fuz}} + \mathbf{u}^{\mathrm{rb}} \right). \tag{29}$$

The block diagram of the proposed saturation-tolerant adaptive control structure is presented in Fig. 3. As shown in Fig. 3, the vectors $\hat{\boldsymbol{\Psi}} = \left[\hat{\Psi}_1, \hat{\Psi}_2, \hat{\Psi}_3\right]^{\mathrm{T}}$ and $\hat{\mathbf{b}} = \left[\hat{\mathbf{b}}_1^{\mathrm{T}}, \hat{\mathbf{b}}_2^{\mathrm{T}}, \hat{\mathbf{b}}_3^{\mathrm{T}}\right]^{\mathrm{T}}$ and the matrix $\hat{\boldsymbol{\gamma}}$ are computed by the block of "Adaptation Laws" representing (26) to (28). The vector $\hat{\boldsymbol{\beta}}^{\mathrm{fuz}}$ is obtained by the block of "Fuzzy Approximator" constructed based on (24). Moreover, by means of (25), the block of "Robust Term" computes the vector $\mathbf{u}^{\mathrm{rb}}$.

Remark 1. The performance of the proposed direct AFSMC in tracking tasks is influenced by the values of α_{1i}, α_{2i}, and α_{3i} and the elements of the matrix $\boldsymbol{\lambda}$. Hence, to tune the controller, $\boldsymbol{\lambda}$, α_{1i}, α_{2i}, and α_{3i} are selected based on the trial-and-error method.

Remark 2. In [28], to implement the direct AFSMC, Levant's exact differentiator was employed for velocity estimation of the microrobot. However, the use of Levant's exact differentiator instead of the first-order derivative increases the computational cost. Since the proposed saturation-tolerant AFSMC is designed with higher number of adaptive variables, we utilize the first-order derivative in the experimental tests as the velocity estimator of the microrobot.

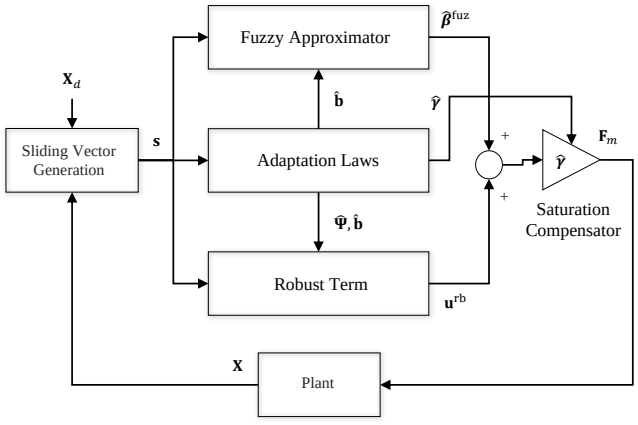

Figure 3: The block diagram of the AFSMC

B. Stability analysis

In the following to the design of the saturation-tolerant AFSMC, the stability analysis of the closed-loop system should be provided based on the definition of Problem 1. For this purpose, Theorem 1 is presented as follows.

Theorem 1. Consider the dynamic behavior of the microrobot described by (1). With the control inputs designed as in (23), where the adaptive variables are adjusted by (26) to (28), then the control objective is achieved according to Problem 1.

Proof. Based on (10) and approximation errors $\tilde{\mathbf{b}}_i = \mathbf{b}_i^* - \hat{\mathbf{b}}_i$, $\tilde{\Psi}_i = \Psi_i - \hat{\Psi}_i$, and $\tilde{\gamma}_i = \vartheta_i - \frac{1}{\hat{\gamma}_i}$, the positive definite function V is defined as follows.

$$V = V_1 + \sum_{i=1}^{3} \frac{1}{2\alpha_{1i}} \tilde{\mathbf{b}}_i^{\mathrm{T}} \tilde{\mathbf{b}}_i + \sum_{i=1}^{3} \frac{1}{2\alpha_{2i}} \tilde{\Psi}_i^2 + \sum_{i=1}^{3} \frac{1}{2\alpha_{3i}} \tilde{\gamma}_i^2 \tag{30}$$

Using (15), the time derivative of V is obtained as

$$\dot{V} = \sum_{i=1}^{3} s_i (\beta_i^* - \theta_i F_{mi}) + \sum_{i=1}^{3} \frac{\tilde{\mathbf{b}}_i^{\mathrm{T}} \dot{\tilde{\mathbf{b}}}_i}{\alpha_{1i}} + \sum_{i=1}^{3} \frac{\tilde{\Psi}_i \dot{\tilde{\Psi}}_i}{\alpha_{2i}} + \sum_{i=1}^{3} \frac{\tilde{\gamma}_i \dot{\tilde{\gamma}}_i}{\alpha_{3i}}. \tag{31}$$

According to

$$\dot{\tilde{\mathbf{b}}}_i = -\dot{\hat{\mathbf{b}}}_i = -\alpha_{1i} s_i \mathbf{w}_i, \tag{32}$$

$$\dot{\tilde{\Psi}}_i = -\dot{\hat{\Psi}}_i = -\alpha_{2i} |s_i|, \tag{33}$$

$$\dot{\tilde{\gamma}}_i = \hat{\gamma}_i^{-2} \dot{\hat{\gamma}}_i = \alpha_{3i} \hat{\gamma}_i \left(|s_i| \hat{\Psi}_i + \left| s_i \hat{\mathbf{b}}_i^{\mathrm{T}} \mathbf{w}_i \right| \right), \tag{34}$$

$$\beta_i^* = \mathbf{b}_i^{*\mathrm{T}} \mathbf{w}_i + \psi_i = \tilde{\mathbf{b}}_i^{\mathrm{T}} \mathbf{w}_i + \hat{\mathbf{b}}_i^{\mathrm{T}} \mathbf{w}_i + \psi_i, \tag{35}$$

and (23) to (28), $\dot{V}$ is rewritten in the form of

$$\begin{aligned} \dot{V} = & \sum_{i=1}^{3} s_i \left(\tilde{\mathbf{b}}_i^{\mathrm{T}} \mathbf{w}_i + \hat{\mathbf{b}}_i^{\mathrm{T}} \mathbf{w}_i + \psi_i \right) - \sum_{i=1}^{3} s_i \theta_i \hat{\gamma}_i \hat{\mathbf{b}}_i^{\mathrm{T}} \mathbf{w}_i \\ & - \sum_{i=1}^{3} \theta_i \hat{\gamma}_i \left(\hat{\Psi}_i + 2 \left| \hat{\mathbf{b}}_i^{\mathrm{T}} \mathbf{w}_i \right| \right) |s_i| \\ & - \sum_{i=1}^{3} s_i \tilde{\mathbf{b}}_i^{\mathrm{T}} \mathbf{w}_i - \sum_{i=1}^{3} (\Psi_i - \hat{\Psi}_i) |s_i| \\ & + \sum_{i=1}^{3} (\hat{\gamma}_i \vartheta_i - 1) |s_i| \hat{\Psi}_i + \sum_{i=1}^{3} (\hat{\gamma}_i \vartheta_i - 1) \left| s_i \hat{\mathbf{b}}_i^{\mathrm{T}} \mathbf{w}_i \right| \end{aligned} \tag{36}$$

which can be simplified as

$$\begin{aligned} \dot{V} = & \sum_{i=1}^{3} \left(s_i \hat{\mathbf{b}}_i^{\mathrm{T}} \mathbf{w}_i + s_i \psi_i \right) - \sum_{i=1}^{3} s_i \theta_i \hat{\gamma}_i \hat{\mathbf{b}}_i^{\mathrm{T}} \mathbf{w}_i \\ & - \sum_{i=1}^{3} \theta_i \hat{\gamma}_i \left(\hat{\Psi}_i + 2 \left| \hat{\mathbf{b}}_i^{\mathrm{T}} \mathbf{w}_i \right| \right) |s_i| - \sum_{i=1}^{3} \Psi_i |s_i| \\ & + \sum_{i=1}^{3} \hat{\gamma}_i \vartheta_i |s_i| \hat{\Psi}_i + \sum_{i=1}^{3} (\hat{\gamma}_i \vartheta_i - 1) \left| s_i \hat{\mathbf{b}}_i^{\mathrm{T}} \mathbf{w}_i \right|. \end{aligned} \tag{37}$$

Since

$$s_i \psi_i \leq |s_i| |\psi_i|, \tag{38}$$

$$s_i \hat{\mathbf{b}}_i^{\mathrm{T}} \mathbf{w}_i \leq \left| s_i \hat{\mathbf{b}}_i^{\mathrm{T}} \mathbf{w}_i \right|, \tag{39}$$

and $\hat{\gamma}_i$ and $\hat{\Psi}_i$ are always positive based on (27), (28), $\hat{\gamma}_i(0) > 0$, and $\hat{\Psi}_i(0) > 0$, it is outlined that

$$\begin{aligned}\dot{V} \leq & \sum_{i=1}^{3}\left(\left|s_i\hat{\mathbf{b}}_i^{\mathrm{T}}\mathbf{w}_i\right| + |s_i||\psi_i|\right) + \sum_{i=1}^{3}\theta_i\hat{\gamma}_i\left|s_i\hat{\mathbf{b}}_i^{\mathrm{T}}\mathbf{w}_i\right| \\ & - \sum_{i=1}^{3}\theta_i\hat{\gamma}_i\left(\hat{\Psi}_i + 2\left|\hat{\mathbf{b}}_i^{\mathrm{T}}\mathbf{w}_i\right|\right)|s_i| - \sum_{i=1}^{3}\Psi_i|s_i| \\ & + \sum_{i=1}^{3}\hat{\gamma}_i\vartheta_i|s_i|\hat{\Psi}_i + \sum_{i=1}^{3}(\hat{\gamma}_i\vartheta_i - 1)\left|s_i\hat{\mathbf{b}}_i^{\mathrm{T}}\mathbf{w}_i\right| \\ = & \sum_{i=1}^{3}|s_i|\left(|\psi_i| - \Psi_i\right) + \sum_{i=1}^{3}\hat{\gamma}_i|s_i|\hat{\Psi}_i(\vartheta_i - \theta_i) \\ & + \sum_{i=1}^{3}\hat{\gamma}_i\left|s_i\hat{\mathbf{b}}_i^{\mathrm{T}}\mathbf{w}_i\right|(\vartheta_i - \theta_i)\end{aligned} \tag{40}$$

Furthermore, based on the assumption $0 < \vartheta_i \leq \theta_i \leq 1$,

$$\sum_{i=1}^{3}\hat{\gamma}_i|s_i|\hat{\Psi}_i(\vartheta_i - \theta_i) \leq 0 \tag{41}$$

and

$$\sum_{i=1}^{3}\hat{\gamma}_i\left|s_i\hat{\mathbf{b}}_i^{\mathrm{T}}\mathbf{w}_i\right|(\vartheta_i - \theta_i) \leq 0. \tag{42}$$

Consequently,

$$\dot{V} \leq \sum_{i=1}^{3}|s_i|\left(|\psi_i| - \Psi_i\right) \leq 0 \tag{43}$$

and the elements of $\mathbf{s}$, $\tilde{\mathbf{\Psi}} = \left[\tilde{\Psi}_1, \tilde{\Psi}_2, \tilde{\Psi}_3\right]^{\mathrm{T}}$, $\tilde{\mathbf{b}} = \left[\tilde{\mathbf{b}}_1^{\mathrm{T}}, \tilde{\mathbf{b}}_2^{\mathrm{T}}, \tilde{\mathbf{b}}_3^{\mathrm{T}}\right]^{\mathrm{T}}$, and $\tilde{\gamma} = \mathrm{diag}(\tilde{\gamma}_1, \tilde{\gamma}_2, \tilde{\gamma}_3)$ remain bounded. It is worth noting that, due to the boundedness of $\dot{\mathbf{s}}$ on the basis of (9), the sliding vector $\mathbf{s}$ is uniformly continuous for $t \geq 0$.

In the next step, the asymptotic stability of the closed-loop system is proved based on Barbalat's lemma. For this purpose, the function Γ is defined in the form of

$$\Gamma = \sum_{i=1}^{3}|s_i|\left(-|\psi_i| + \Psi_i\right). \tag{44}$$

Hence, according to (44), (43) is rewritten as

$$\dot{V} \leq -\Gamma \leq 0 \tag{45}$$

and the following inequality is obtained.

$$\Gamma \leq -\dot{V} \tag{46}$$

By integrating (46) with respect to time, we have

$$\int_0^t \Gamma(\tau)d\tau \leq V(\mathbf{s}, \tilde{\mathbf{b}}, \tilde{\mathbf{\Psi}}, \tilde{\gamma})|_{\tau=0} - V(\mathbf{s}, \tilde{\mathbf{b}}, \tilde{\mathbf{\Psi}}, \tilde{\gamma})|_{\tau=t}. \tag{47}$$

Because $\dot{V} \leq 0$, the value of $V(\mathbf{s}, \tilde{\mathbf{b}}, \tilde{\mathbf{\Psi}}, \tilde{\gamma})|_{\tau=t}$ does not increase over time. In consequence, due to the boundedness of $V(\mathbf{s}, \tilde{\mathbf{b}}, \tilde{\mathbf{\Psi}}, \tilde{\gamma})|_{\tau=0}$ and $V(\mathbf{s}, \tilde{\mathbf{b}}, \tilde{\mathbf{\Psi}}, \tilde{\gamma})|_{\tau=t}$, $\lim_{t\to\infty}\int_0^t \Gamma(\tau)d\tau$ is also bounded. Moreover, since Γ is continuous in bounded variables s_i, Γ is uniformly continuous in t on $(0, +\infty)$. Consequently, according to Barbalat's lemma [37], $\lim_{t\to\infty}\Gamma(t) = 0$, i.e., $\lim_{t\to\infty}\mathbf{s}(t) = 0$.

Remark 3. To diminish chattering effects caused by the robust compensators u_i^{rb}, the signum function $\mathrm{sgn}(s_i)$ is replaced by a saturation function. Thus, since the closed-loop system is asymptotically stable, the sliding variables s_i reach the boundary layer of the saturation function.

IV. Experimental Study

In this study, the electromagnetic manipulation system built in the lab has been employed to investigate the performance of the proposed direct AFSMC. As shown in Fig. 4, the utilized system contains eight electromagnetic coils for generating an intended magnetic field in the working area [38]. Moreover, the dimensions of the uniform workspace is $16\ \mathrm{mm} \times 16\ \mathrm{mm} \times 12\ \mathrm{mm}$. The microrobot is a cylindrical Neodymium magnet

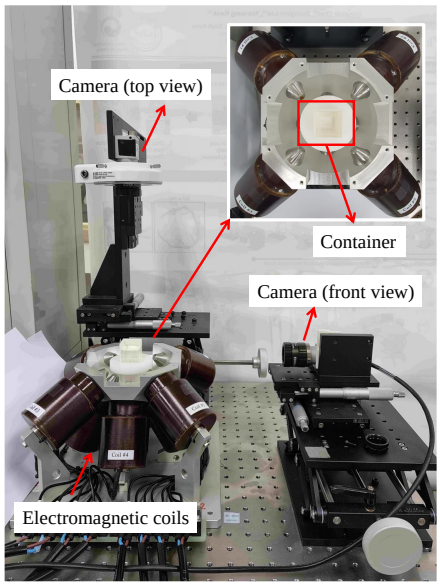

Figure 4: Experimental setup of the magnetic control system

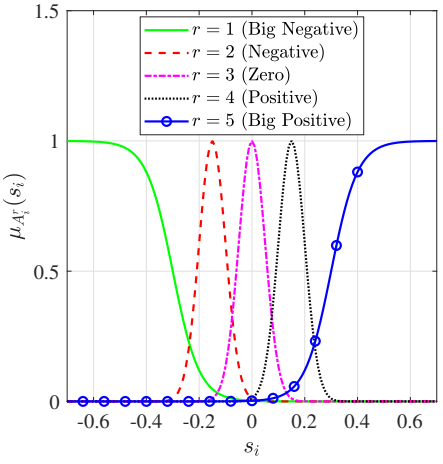

Figure 5: The membership functions proposed for the fuzzy sets A_i^r

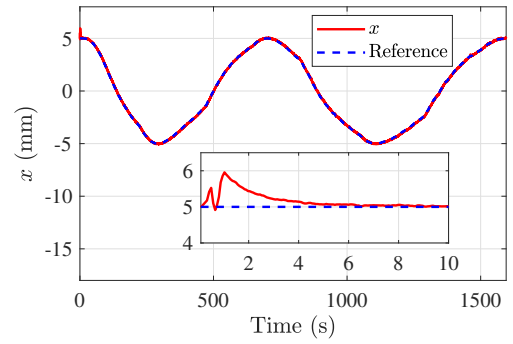

(a)

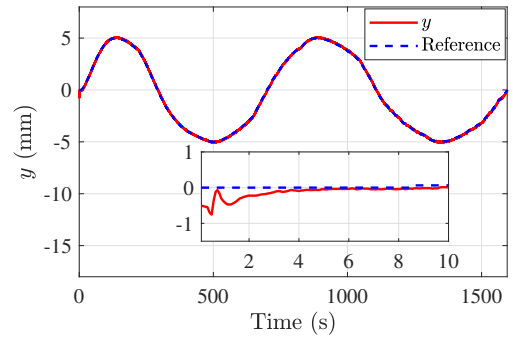

(b)

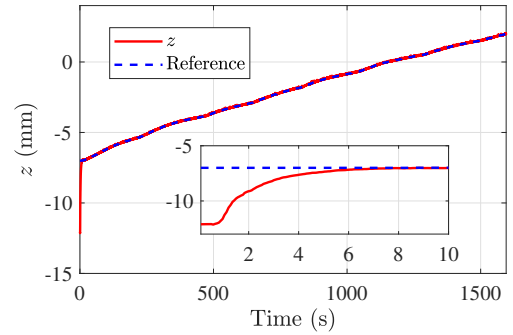

(c)

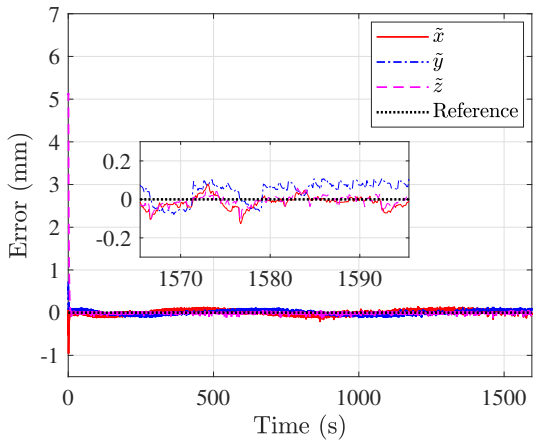

(d)

Figure 6: Time evolution of (a) x, (b) y, (c) z, and (d) the tracking errors in the case of using the anti-windup-based TDC and choosing the spiral reference path

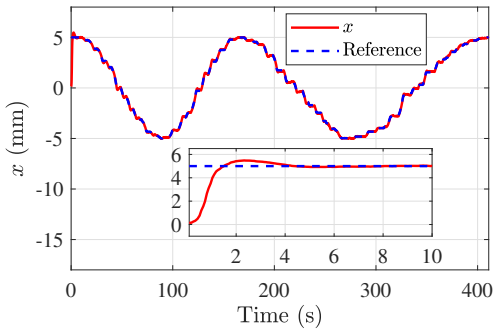

(a)

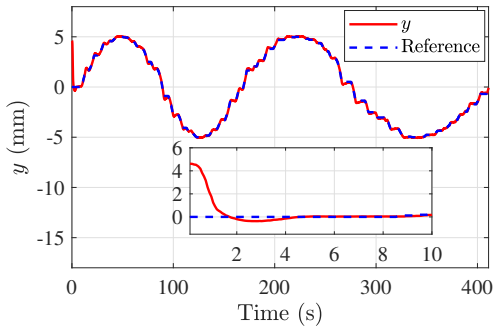

(b)

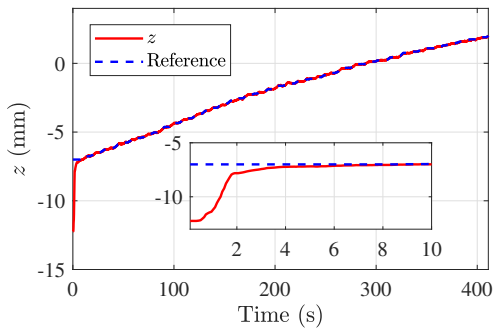

(c)

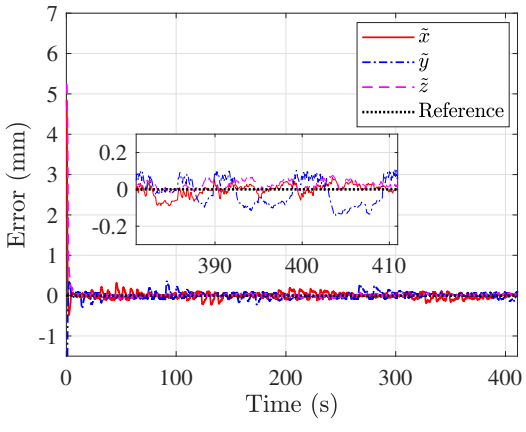

(d)

Figure 7: Time evolution of (a) x, (b) y, (c) z, and (d) the tracking errors in the case of using the proposed AFSMC and choosing the spiral reference path

with a length of 800 μm and a diameter of 400 μm which has been submerged in Silicone oil of 350-cSt viscosity in a transparent container. To simulate the in vivo situation reported in [39], we used high-viscosity silicone oil as the medium for the control problem of the microrobot with high magnetic moment. In the in vivo situation of [39], a biocompatible microrobot with low magnetic moment (0.017×10^{-6} A.m^2) swims in blood of 10-cSt viscosity. Furthermore, the position of the microrobot is measured by the two cameras. The employed cameras are ACA1300-30um, Basler AG (Germany), where every frame is of resolution 966×966 pixels. The scale of every frame is 29 μm/pixel and the framerate has been chosen equal to 15 Hz, same as the sampling frequency of the AFSMC loop.

In addition to the above-mentioned notes, $F_{m,\min} = -50$ μN, $F_{m,\max} = 50$ μN, $||\mathbf{M}|| = 0.00027$ A.m^2 for the Neodymium magnet [27], $\mathbf{B} = [0, 0, 5]^{\mathrm{T}}$ mT, and the matrix $\mathbf{K}$ was computed with the use of the magnetometer THM1176 (Metrolab Technology SA, Plan-les-Ouates, Switzerland) which has been employed for measuring the magnetic field vectors at the center of the working area. Since the experiments are conducted on the basis of the constant vector $\mathbf{B}$, it is allowed to claim (4) as an assumption and obtain the magnetic force vector $\mathbf{F}_m$ by using (6).

In order to implement the designed AFSMC, the constant parameters have been selected as $\boldsymbol{\lambda} = \mathrm{diag}(50, 50, 50)$, $\mathbf{c}_i = [-0.3, -0.15, 0, 0.15, 0.3]^{\mathrm{T}}$, $\boldsymbol{\sigma}_i = [-0.05, 0.05, 0.05, 0.05, 0.05]^{\mathrm{T}}$, $\alpha_{1i} = 10^{-4}$, $\alpha_{2i} = 2.5 \times 10^{-4}$, and $\alpha_{3i} = 10^{-5}$. According to the selected vectors $\mathbf{c}_i$ and $\boldsymbol{\sigma}_i$, the membership functions of the fuzzy sets A_i^r are generated as in Fig. 5. It is worth noting that, based on the proof of Theorem 1, the asymptotic stability of the closed-loop system is not dependent on the values of $\mathbf{c}_i$ and $\boldsymbol{\sigma}_i$. Hence, users are allowed to implement the proposed AFSMC with the help of arbitrary vectors $\mathbf{c}_i$ and $\boldsymbol{\sigma}_i$ in a meaningful range of s_i. In addition, the initial condition of the adaptive variables have been chosen as $\hat{\gamma}_i(0) = 1$, $\hat{\mathbf{b}}_i(0) = [-10^{-6}, -5 \times 10^{-7}, 0, 5 \times 10^{-7}, 10^{-6}]^{\mathrm{T}}$, and $\hat{\Psi}_i(0) = 10^{-6}$.

In this article, the experimental study for the performance evaluation of the proposed AFSMC has been conducted for two test scenarios. In the first scenario, the magnetic forces must be generated in a way that the microrobot tracks a spiral reference path. Moreover, the performance of the proposed AFSMC is compared with that of the anti-windup-based TDC [19] as a state-of-the-art method. It is important to note that, to track the desired postion smoothly, the reference path has been generated as a combination of 1000 setpoints. In other words, if the microrobot reaches a certain distance from each setpoint,

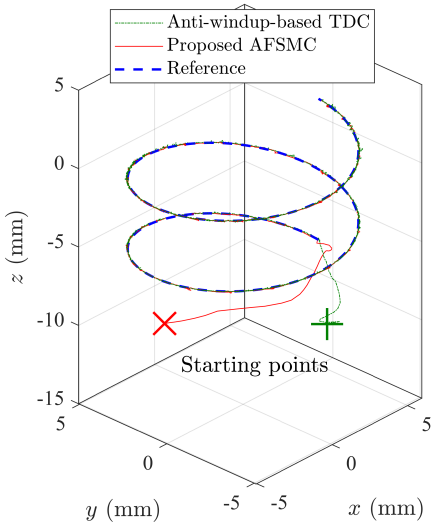

Figure 8: The 3D microrobot's position graph under the anti-windup-based TDC and the proposed AFSMC in the case of choosing the spiral reference path

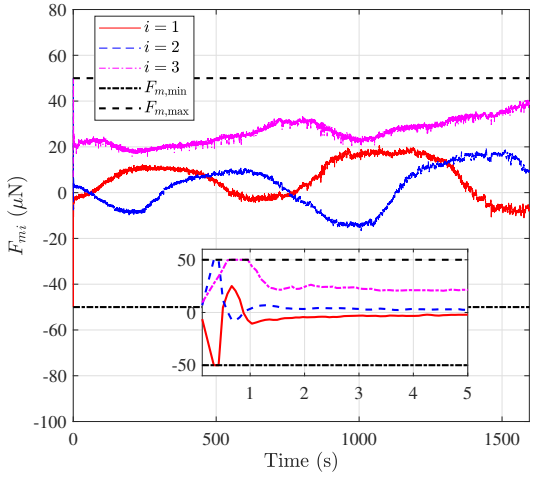

(a)

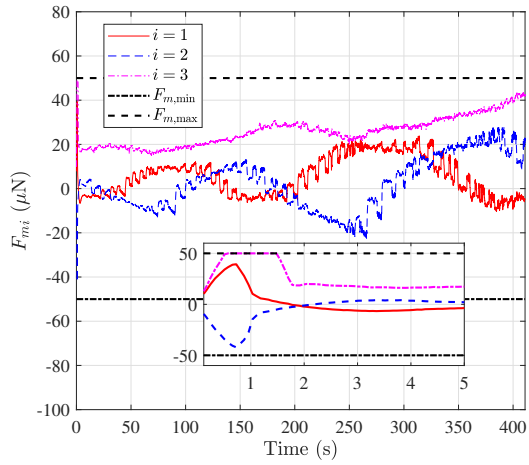

(b)

Figure 9: Time evolution of the control inputs F_{mi} $(i = 1, 2, 3)$ generated by (a) the anti-windup-based TDC and (b) the proposed AFSMC in the case of choosing the spiral reference path

which is called the threshold, then the microrobot has to move toward the next setpoint. In addition, the threshold should be determined based on the time constant of the electromagnetic manipulation system via the trial-and-error method. In this experiment, the threshold is chosen to be equal to 0.05 mm.

The experimental results corresponding to the first test are presented in Fig. 6 to Fig. 9. As it is illustrated in Fig. 6 and Fig. 7, by means of the anti-windup-based TDC and the proposed AFSMC, the microrobot has successfully tracked the reference trajectories in x, y, and z directions where the magnitudes of the tracking errors $\tilde{x}$, $\tilde{y}$, and $\tilde{z}$ in the last 30 seconds of motion were less than 0.2 mm. Furthermore, the 3D graphs of the microrobot position under the anti-

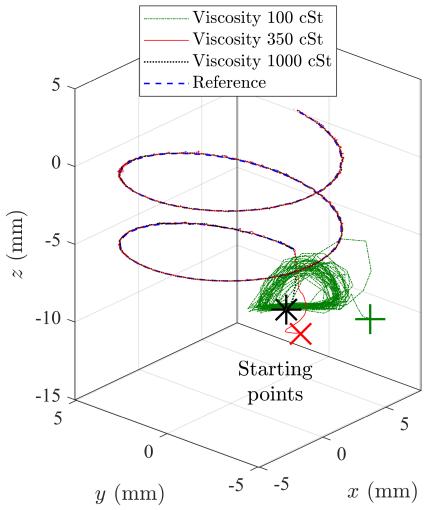

(a)

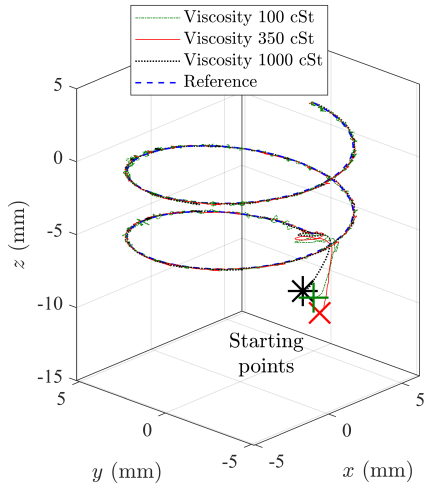

(b)

Figure 10: The 3D microrobot's position graph for different values of viscosity under (a) the anti-windup-based TDC and (b) the proposed AFSMC in the case of choosing the spiral reference path

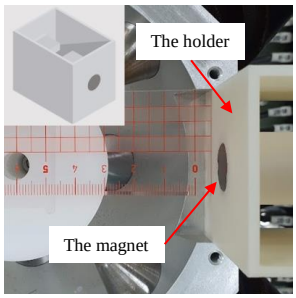

(a)

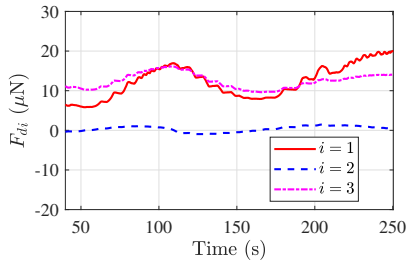

(b)

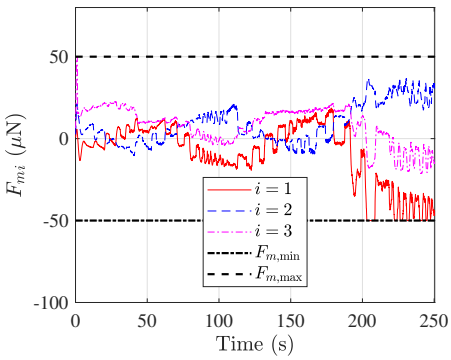

(c)

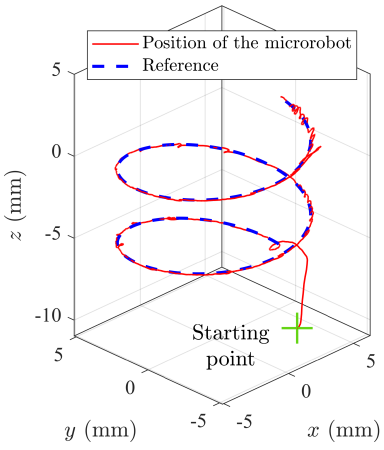

(d)

Figure 11: Control of the microrobot using the proposed AFSMC in the presence of an external disturbance. (a) The external magnet placed in the holder. (b) The disturbances F_{di} $(i = 1, 2, 3)$ vesus time. (c) The inputs F_{mi} $(i = 1, 2, 3)$ versus time. (d) The 3D microrobot's position graph.

windup-based TDC and the proposed AFSMC have been presented in Fig. 8. According to Fig. 8, after approaching to the reference trajectory from different starting points, the 3D graphs corresponding the two methods have been almost identical. The most important point is that the comparison of the completion times shows that the proposed AFSMC can track the desired trajectory considerably faster than the anti-windup-based TDC. In continuation, time evolution of the control inputs F_{mi} $(i = 1, 2, 3)$ generated by the two methods have been shown in Fig. 9. As it is seen in Fig. 9 (b), F_{m3} corresponding to the proposed AFSMC has been saturated during the first two seconds of the motion. Since the tracking of the reference trajectory in z direction has not been influenced by the saturation of F_{m3}, it can be claimed that the proposed AFSMC has compensated for the effects of the input saturation. It should be noted that, as shown in Fig. 9 (a), implementation of the anti-windup-based TDC has caused the saturation of all the control inputs (F_{mi} $(i = 1, 2, 3)$).

It should be noted that the magnitudes of the tracking errors $\tilde{x}$, $\tilde{y}$, and $\tilde{z}$ and the completion time are dependent on the value of the threshold. In continuation, for different values of threshold and using the anti-windup-based TDC and the proposed AFSMC, the completion time and the maximum of $|\tilde{x}|$, $|\tilde{y}|$, and $|\tilde{z}|$ after $t = 14$ s are presented in Table I. It is worth noting that, to better evaluate the performance of the two methods in tracking, the magnitudes of the tracking errors have been reported after approaching the spiral reference path (after $t = 14$ s). According to the results provided in Table I, by increasing the value of the threshold in the implementation of the two methods, the completion time of the mission is decreased. However, increase of the threshold causes tracking performance degradation. As a result, with the help of changing the threshold, the velocity of movement can be tuned.

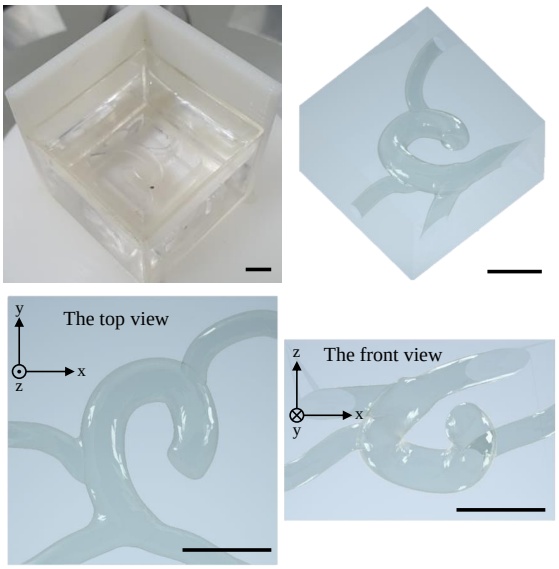

Figure 12: The 3D printed Aorta phantom (All scale bars correspond to 5 mm.)

It should be emphasized that the proposed AFSMC has been successful in significantly decreasing the completion time for all threshold values. From another point of view, by using the proposed AFSMC, the maximum absolute value of the tracking errors has been increased for each threshold compared to the anti-windup-based TDC. For instance, for the threshold equal to 0.05 mm, the maximum of $|\tilde{x}|$, $|\tilde{y}|$, and $|\tilde{z}|$ has been increased 75.7324 %. On the other hand, with the help of the proposed AFSMC implemented based on the threshold of 0.05 mm, the completion time has reduced 74.2426 %. It is noteworthy that, according to Fig. 6 (d) and Fig. 7 (d), the values of $|\tilde{x}|$, $|\tilde{y}|$, and $|\tilde{z}|$ in the last 30 seconds of motion

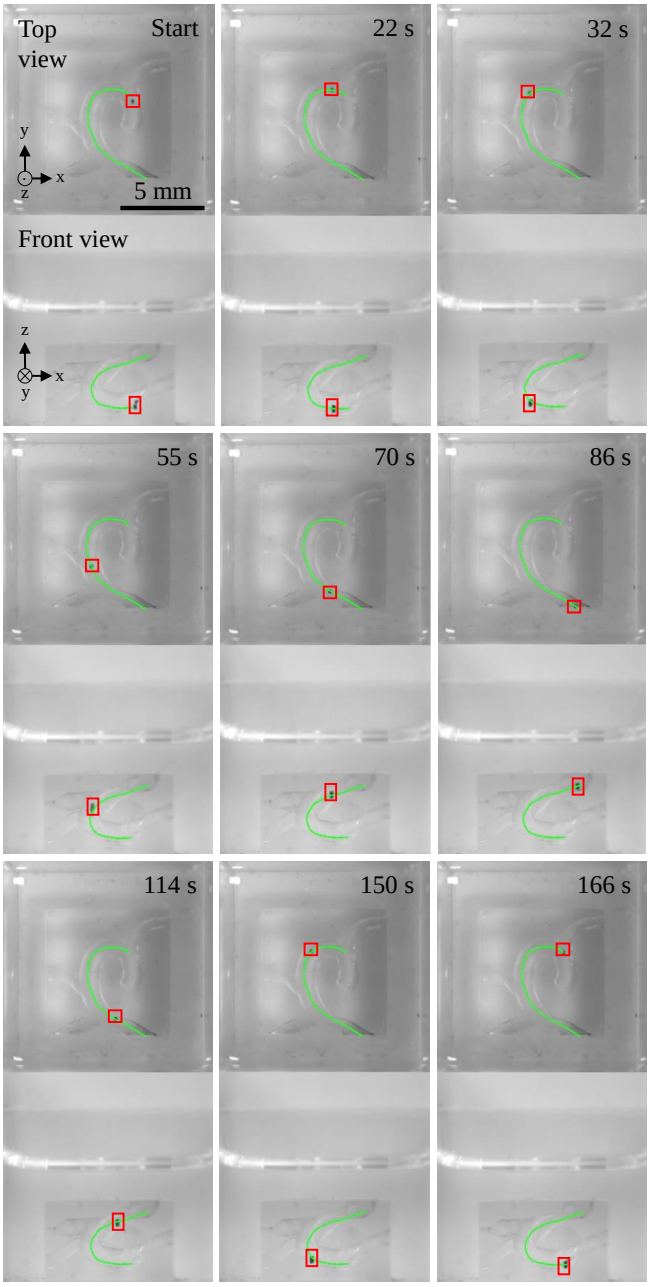

Figure 13: Captured images of the microrobot manipulation inside the phantom

were less than 0.2 mm. Also, in this comparative analysis, to implement the anti-windup-based TDC, it is assumed that the mass of the microrobot is known. As has been studied in [28], the performance of the anti-windup-based TDC is highly dependent on the nominal mass matrix set by the user. In other words, if the nominal value of the mass is chosen far from the real value, the performance of the anti-windup-based TDC will be degraded significantly.

In order to evaluate the robustness of the controller in different experimental conditions, the anti-windup-based TDC and the proposed AFSMC have also been tested in Silicone oils with 100-cSt and 1000-cSt viscosities. It is worth noting that both the controllers have been tuned based on the trial-and-error in the Silicone oil of 350-cSt viscosity. The experimental results obtained for different mediums in tracking the spiral trajectory with the threshold of 0.1 mm have been presented in Fig. 10 and Table II. According to Fig. 10, the proposed AFSMC has been successful in tracking the desired trajectory even with the change of the medium. However, in the case of testing in Silicone oil of 100-cSt, the anti-windup-based TDC failed to track the reference path. It is worth noting that, as reported in Table II, with the increase of the viscosity, the completion time and the maximum of $|\tilde{x}|$, $|\tilde{y}|$, and $|\tilde{z}|$ corresponding to the proposed AFSMC have increased.

In continuation, to induce external disturbances in the system, we selected a Neodymium N52 cylindrical magnet with dimensions of 30 mm in length and 15 mm in diameter. This magnet was placed in a 3D-printed holder (see Fig. 11 (a)) for convenient alignment and assembly with the magnetic actuation system. Positioned at $\mathbf{X} = [65, 0, 0]^{\mathrm{T}}$ mm, the magnet was affixed with its north pole facing inward towards the $+x$-axis. This placement occurred at approximately $t = 40$ s during tracking in the Silicone oil of 350-cSt viscosity and time evolution of the force disturbances F_{di} $(i = 1, 2, 3)$ have been presented in Fig. 11 (b). The external magnetic forces have been estimated by the Dipole model [40] and verified with a FEM simulation in COMSOL. The calculations show that the microrobot faced a maximum disturbance of 20 μN in the x-direction $(i = 1)$.

The control inputs F_{mi} $(i = 1, 2, 3)$ generated by the proposed AFSMC and the 3D microrobot's position graph in the presence of the external magnet have been shown in Fig. 11 (c) and Fig. 11 (d), respectively. As is seen in Fig. 11 (c), the compensation of the disturbance force F_{d1} has caused the saturation of F_{m1} after $t = 200$ s. Nevertheless, according to Fig. 11 (d), the microrobot has autonomously tracked the spiral reference path with the threshold of 0.1 mm. Hence, this test shows that the proposed AFSMC is also capable of compensating for the effects of external disturbances.

In the second test scenario, with the aim of providing a more realistic example, the electromagnetic manipulation system has been employed to control the position of the microrobot in the simplified Aorta phantom shown in Fig. 12. The Aorta is a large and cane-shaped vessel delivering oxygen-rich blood to the body [38], [41]. The 3D printed Aorta phantom that we use was made identical to the heart of a human with reduced number of branches, scaled down to roughly the size of a mouse's heart. The maximum and minimum diameters of the vessels are 2.5 mm and 1.5 mm, respectively. Moreover, the footprint of the phantom is 15 mm $\times$ 15 mm $\times$ 10 mm. The phantom has been 3D printed by Logical Design (Gyeonggi-do, South Korea) using the SLA method. The material used is Accura ClearVue and the printer employed is called ProX 800.

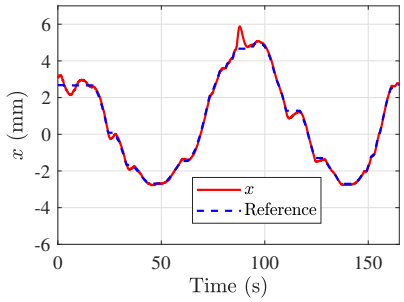

(a)

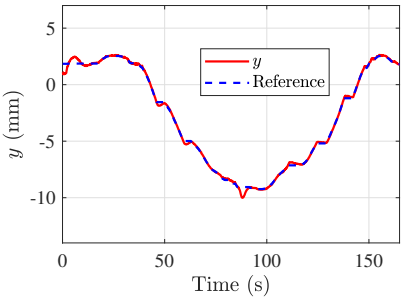

(b)

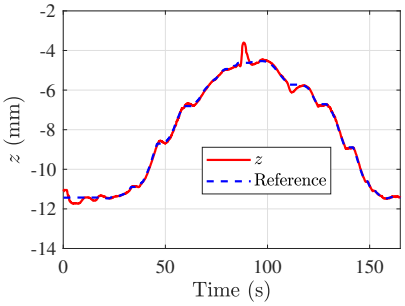

(c)

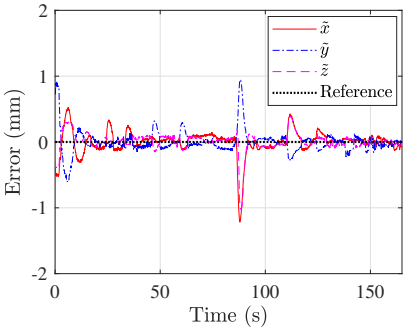

(d)

Figure 14: Time evolution of (a) x, (b) y, (c) z, and (d) the tracking errors corresponding to the phantom experiment scenario

Table I: Performance comparison of the anti-windup-based TDC and the proposed AFSMC in tracking the spiral trajectory

Threshold [mm]	Maximum of $\|\tilde{x}\|$, $\|\tilde{y}\|$, and $\|\tilde{z}\|$ after $t = 14$ s [mm]			Completion time [s]		
	Anti-windup-based TDC	Proposed AFSMC	Percentage change	Anti-windup-based TDC	Proposed AFSMC	Percentage change
0.05	0.2054	0.3610	75.7324 %	1595.5	410.9553	-74.2426 %
0.10	0.2204	0.4774	116.6140 %	896.9193	249.7678	-72.1527 %
0.15	0.2290	0.5497	140.0177 %	624.5330	177.2086	-71.6254 %
0.20	0.2721	0.5827	114.1450 %	490.4476	153.7078	-68.6597 %
0.30	0.3637	0.6831	87.7888 %	330.5236	118.7852	-64.0615 %

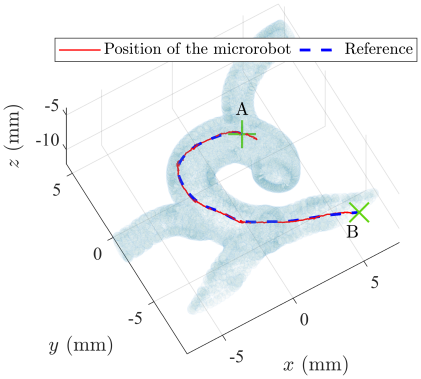

(a)

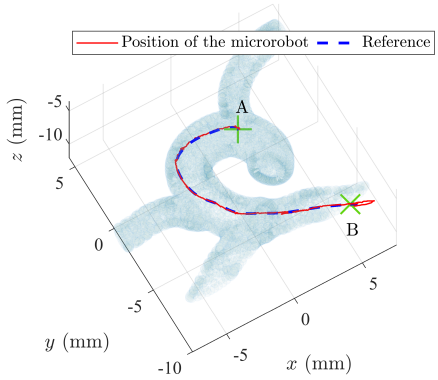

(b)

Figure 15: The 3D microrobot's position graph in the phantom experiment scenario when tracking the reference trajectory (a) from A to B and (b) from B to A

Before starting the experiment, the phantom was placed inside the Silicone oil 350-cSt, and then placed inside the vacuum to eliminate the air bubbles. The results corresponding to the phantom experiment scenario under the proposed AFSMC with the threshold of 0.1 mm are shown in Fig. 13 to Fig. 16. As it was expected, Fig. 13 to Fig. 15 reveal that the saturation-tolerant AFSMC can track the reference path successfully in the second experiment scenario. According to

Table II: Performance comparison of the proposed AFSMC for different values of viscosity in tracking the spiral trajectory with the threshold of 0.1 mm

Viscosity [cSt]	Maximum of $\|\tilde{x}\|$, $\|\tilde{y}\|$, and $\|\tilde{z}\|$ after $t = 14$ s [mm]	Completion time [s]
100	0.3336	223.5391
350	0.4774	249.7678
1000	0.4836	384.1903

Fig. 14 (d), the minimum and the maximum values of the tracking errors are -1.22 mm and 0.95 mm, repectively. As shown in Fig. 16, since the initial position of the microrobot was near the reference starting point A, the generated control inputs F_{mi} $(i = 1, 2, 3)$ have not been saturated for the first few seconds. It should be noted that, in the second experiment scenario, the microrobot has tracked a path to reach the reference destination point B and then returned toward the reference starting point A. Hence, at the time of changing the direction (near $t = 86$ s), the overshoots in x and z and the undershoot in y have been appeared (see Fig. 14). As supplementary materials, videos S1, S2, S3, and S4 have been provided to show the microrobot control in the first and

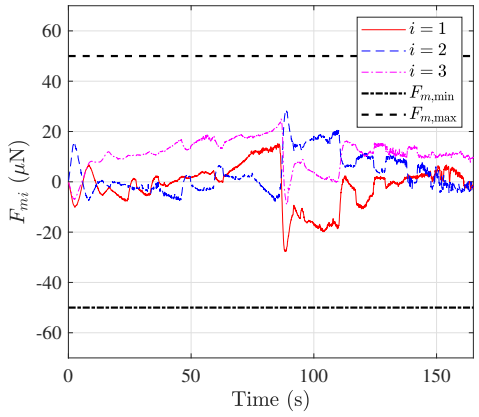

Figure 16: The generated control inputs F_{mi} $(i = 1, 2, 3)$ versus time corresponding to the phantom experiment scenario

second test scenarios. Moreover, the FEM simulation results corresponding to the external magnet have been provided in the supplementary material S5.

V. Conclusions

In this article, an input saturation-tolerant adaptive fuzzy sliding-mode control scheme has been designed to provide a model-free approach for the position control of the magnetic microrobots. Each AFSMC input consists of a fuzzy inference term utilized to approximate an unknown nonlinear function including uncertain forces, a robust part derived to compensate for the fuzzy approximation error and disturbances, and a saturation compensating gain. The presented control method can be implemented without prior information about the physical properties of the fluid and the microrobot. Furthermore, the proposed control structure does not face the limitations of the anti-windup-based TDC and previous direct AFSMC methods. The stability of the control system with the possibility of input saturation has been proved.

To evaluate the performance of the proposed AFSMC, two experimental scenarios have been proposed. The experimental results corresponding to the spiral reference path reveal that the magnitudes of the tracking errors were less than 0.2 mm at the end of the motion. Moreover, in the phantom experiment scenario, the minimum and the maximum values of the tracking errors were -1.22 mm and 0.95 mm, respectively. Hence, in both scenarios, it can be claimed that the saturation-tolerant AFSMC has tracked the reference path successfully. In addition to the above-mentioned notes, compared to the anti-windup-based TDC, the proposed AFSMC has been successful in significantly decreasing the completion time and improving the tracking performance with the change of the medium.

It is important to note that the proposed control method has been designed with no dependency on the shape of the microrobot. However, the range of the tracking errors may be affected by changing the microrobot's shape. Hence, to obtain the best possible performance, the tuning of the controller's parameters should be repeated for each microrobot geometry. Since it is of high importance to guarantee that the microrobot does not collide with the walls of veins, the AFSMC method can be developed for the collision avoidance problem in future works. Moreover, designing the AFSMC based on a guaranteed precision will have a great impact in related applications.

References

[1] S. Jeon, A. K. Hoshiar, K. Kim, S. Lee, E. Kim, S. Lee, J. young Kim, B. J. Nelson, H.-J. Cha, B.-J. Yi, and H. Choi, "A magnetically controlled soft microrobot steering a guidewire in a three-dimensional phantom vascular network," *Soft Robotics*, vol. 6, pp. 54–68, 2 2019.

[2] P. Lloyd, A. K. Hoshiar, T. da Veiga, A. Attanasio, N. Marahrens, J. H. Chandler, and P. Valdastri, "A learnt approach for the design of magnetically actuated shape forming soft tentacle robots," *IEEE Robotics and Automation Letters*, vol. 5, pp. 3937–3944, 7 2020.

[3] D. Li, H. Choi, S. Cho, S. Jeong, Z. Jin, C. Lee, S. Y. Ko, J.-O. Park, and S. Park, "A hybrid actuated microrobot using an electromagnetic field and flagellated bacteria for tumor-targeting therapy," *Biotechnology and Bioengineering*, vol. 112, pp. 1623–1631, 8 2015.

[4] J. Han, J. Zhen, V. D. Nguyen, G. Go, Y. Choi, S. Y. Ko, J.-O. Park, and S. Park, "Hybrid-actuating macrophage-based microrobots for active cancer therapy," *Scientific Reports*, vol. 6, p. 28717, 6 2016.

[5] V. D. Nguyen, V. H. Le, S. Zheng, J. Han, and J.-O. Park, "Preparation of tumor targeting cell-based microrobots carrying nir light sensitive therapeutics manipulated by electromagnetic actuating system and chemotaxis," *Journal of Micro-Bio Robotics*, vol. 14, pp. 69–77, 12 2018.

[6] J. Park, C. Jin, S. Lee, J. Kim, and H. Choi, "Magnetically actuated degradable microrobots for actively controlled drug release and hyperthermia therapy," *Advanced Healthcare Materials*, vol. 8, p. 1900213, 8 2019.

[7] S. Lee, J. Kim, J. Kim, A. K. Hoshiar, J. Park, S. Lee, J. Kim, S. Pané, B. J. Nelson, and H. Choi, "A needle-type microrobot for targeted drug delivery by affixing to a microtissue," *Advanced Healthcare Materials*, vol. 9, p. 1901697, 4 2020.

[8] K. Abolfathi, M. R. H. Yazdi, and A. K. Hoshiar, "Studies of different swarm modes for the mnps under the rotating magnetic field," *IEEE Transactions on Nanotechnology*, vol. 19, pp. 849–855, 2020.

[9] T. Xu, J. Yu, X. Yan, H. Choi, and L. Zhang, "Magnetic actuation based motion control for microrobots: An overview," *Micromachines*, vol. 6, pp. 1346–1364, 9 2015.

[10] K. T. Nguyen, G. Go, E. Choi, B. Kang, J.-O. Park, and C.-S. Kim, "A guide-wired helical microrobot for mechanical thrombectomy: A feasibility study," in *2018 40th Annual International Conference of the IEEE Engineering in Medicine and Biology Society (EMBC)*, 7 2018, pp. 1494–1497.

[11] T. Yamanaka and F. Arai, "Self-propelled swimming microrobot using electroosmotic propulsion and biofuel cell," *IEEE Robotics and Automation Letters*, vol. 3, pp. 1787–1792, 7 2018.

[12] X. Wu, J. Liu, C. Huang, M. Su, and T. Xu, "3-d path following of helical microswimmers with an adaptive orientation compensation model," *IEEE Transactions on Automation Science and Engineering*, vol. 17, pp. 823–832, 4 2020.

[13] T. Xu, Y. Guan, J. Liu, and X. Wu, "Image-based visual servoing of helical microswimmers for planar path following," *IEEE Transactions on Automation Science and Engineering*, vol. 17, pp. 325–333, 1 2020.

[14] A. Hosney, A. Klingner, S. Misra, and I. S. M. Khalil, "Propulsion and steering of helical magnetic microrobots using two synchronized rotating dipole fields in three-dimensional space," in *2015 IEEE/RSJ International Conference on Intelligent Robots and Systems (IROS)*, 9 2015, pp. 1988–1993.

[15] S. Jeon, S. Kim, S. Ha, S. Lee, E. Kim, S. Y. Kim, S. H. Park, J. H. Jeon, S. W. Kim, C. Moon, B. J. Nelson, J. young Kim, S.-W. Yu, and H. Choi, "Magnetically actuated microrobots as a platform for stem cell transplantation," *Science Robotics*, vol. 4, 5 2019.

[16] M. E. Tiryaki, O. Erin, and M. Sitti, "A realistic simulation environment for mri-based robust control of untethered magnetic robots with intra-operational imaging," *IEEE Robotics and Automation Letters*, vol. 5, pp. 4501–4508, 7 2020.

[17] P. B. Nguyen, J.-O. Park, S. Park, and S. Y. Ko, "Medical micro-robot navigation using image processing - blood vessel extraction and x-ray calibration," in *2016 6th IEEE International Conference on Biomedical Robotics and Biomechatronics (BioRob)*, 6 2016, pp. 365–370.

[18] J. Piepmeier, S. Firebaugh, and C. Olsen, "Uncalibrated visual servo control of magnetically actuated microrobots in a fluid environment," *Micromachines*, vol. 5, pp. 797–813, 9 2014.

[19] J. Kim, H. Choi, and J. Kim, "A robust motion control with antiwindup scheme for electromagnetic actuated microrobot using time-delay estimation," *IEEE/ASME Transactions on Mechatronics*, vol. 24, pp. 1096–1105, 6 2019.

[20] M. Khamesee, N. Kato, Y. Nomura, and T. Nakamura, "Design and control of a microrobotic system using magnetic levitation," *IEEE/ASME Transactions on Mechatronics*, vol. 7, pp. 1–14, 3 2002.

[21] H. Marino, C. Bergeles, and B. J. Nelson, "Robust electromagnetic control of microrobots under force and localization uncertainties," *IEEE Transactions on Automation Science and Engineering*, vol. 11, pp. 310–316, 1 2014.

[22] Z. Zhang, F. Long, and C.-H. Menq, "Three-dimensional visual servo control of a magnetically propelled microscopic bead," *IEEE Transactions on Robotics*, vol. 29, pp. 373–382, 4 2013.

[23] L. Mellal, D. Folio, K. Belharet, and A. Ferreira, "Optimal control of multiple magnetic microbeads navigating in microfluidic channels," in *2016 IEEE International Conference on Robotics and Automation (ICRA)*, 5 2016, pp. 1921–1926.

[24] L. Arcese, M. Fruchard, and A. Ferreira, "Adaptive controller and observer for a magnetic microrobot," *IEEE Transactions on Robotics*, vol. 29, pp. 1060–1067, 8 2013.

[25] S. Xu, J. Liu, C. Yang, X. Wu, and T. Xu, "A learning-based stable servo control strategy using broad learning system applied for microrobotic

control," *IEEE Transactions on Cybernetics*, vol. 52, pp. 13 727–13 737, 12 2022.

[26] T. Xu, C. Huang, Z. Lai, and X. Wu, "Independent control strategy of multiple magnetic flexible millirobots for position control and path following," *IEEE Transactions on Robotics*, vol. 38, pp. 2875–2887, 10 2022.

[27] A. Ghanbari, P. H. Chang, B. J. Nelson, and H. Choi, "Magnetic actuation of a cylindrical microrobot using time-delay-estimation closed-loop control: modeling and experiments," *Smart Materials and Structures*, vol. 23, p. 035013, 3 2014.

[28] A. Mousavi, H. Khaksar, A. Ahmed, H. Choi, and A. K. Hoshiar, "Magnetic microrobot control using an adaptive fuzzy sliding-mode method," in *2022 IEEE/RSJ International Conference on Intelligent Robots and Systems (IROS)*, 10 2022, pp. 6484–6489.

[29] H. Navvabi and A. H. D. Markazi, "New afsmc method for nonlinear system with state-dependent uncertainty: Application to hexapod robot position control," *Journal of Intelligent and Robotic Systems*, vol. 95, pp. 61–75, 7 2019.

[30] A. H. D. Markazi, M. Maadani, S. H. Zabihifar, and N. Doost-Mohammadi, "Adaptive fuzzy sliding mode control of under-actuated nonlinear systems," *International Journal of Automation and Computing*, vol. 15, pp. 364–376, 6 2018.

[31] H. Navvabi and A. Markazi, "Position control of stewart manipulator using a new extended adaptive fuzzy sliding mode controller and observer (e-afsmco)," *Journal of the Franklin Institute*, vol. 355, pp. 2583–2609, 3 2018.

[32] A. Mousavi and A. H. D. Markazi, "An adaptive fuzzy sliding-mode control method for leader-follower consensus of uncertain non-square nonlinear systems," *International Journal of Adaptive Control and Signal Processing*, vol. 36, pp. 3230–3253, 12 2022.

[33] A. Mousavi and A. H. Markazi, "A predictive approach to adaptive fuzzy sliding-mode control of under-actuated nonlinear systems with input saturation," *International Journal of Systems Science*, vol. 52, pp. 1599–1617, 2021.

[34] M. P. Kummer, J. J. Abbott, B. E. Kratochvil, R. Borer, A. Sengul, and B. J. Nelson, "Octomag: An electromagnetic system for 5-dof wireless micromanipulation," *IEEE Transactions on Robotics*, vol. 26, pp. 1006–1017, 12 2010.

[35] A. Ghanbari, P. H. Chang, B. J. Nelson, and H. Choi, "Electromagnetic steering of a magnetic cylindrical microrobot using optical feedback closed-loop control," *International Journal of Optomechatronics*, vol. 8, pp. 129–145, 4 2014.

[36] B. Kosko, "Fuzzy systems as universal approximators," *IEEE Transactions on Computers*, vol. 43, pp. 1329–1333, 1994.

[37] J.-J. E. Slotine and W. Li, *Applied Nonlinear Control*. Prentice Hall, 1991.

[38] N. L. Gharamaleki, J. Hwang, A. Ahmed, S. A. Abbasi, S.-I. Kim, J.-Y. Kim, and H. Choi, "Electromagnetic manipulation system for semi-autonomous control of small-scale magnetic objects with sequential programming," *IEEE Access*, vol. 11, pp. 35 327–35 335, 2023.

[39] S. Kim, F. Qiu, S. Kim, A. Ghanbari, C. Moon, L. Zhang, B. J. Nelson, and H. Choi, "Fabrication and characterization of magnetic microrobots for three-dimensional cell culture and targeted transportation," *Advanced Materials*, vol. 25, pp. 5863–5868, 11 2013.

[40] B. Thomaszewski, A. Gumann, S. Pabst, and W. Straßer, "Magnets in motion," *ACM Transactions on Graphics*, vol. 27, pp. 1–9, 12 2008.

[41] C. Rosendorff, Ed., *Essential Cardiology*. Springer New York, 2013.

Alireza Mousavi received his Ph.D. from the School of Mechanical Engineering, Iran University of Science and Technology (IUST), Tehran, Iran, in 2022. He is currently working on the development of intelligent control methods for micro robotic manipulation systems. His research interests include adaptive fuzzy sliding-mode control of nonlinear systems, consensus control of multi-agent dynamical systems, reinforcement learning-based control, and Robotics.

Awais Ahmed received his bachelor's degree in Mechatronics Engineering from National University of Sciences and Technology (NUST), Islamabad, Pakistan in 2017. He then received a master's degree in Robotics Engineering in 2020 from Daegu Gyeongbuk Institute of Science and Technology (DGIST), Daegu, South Korea. Currently, he is pursuing his doctorate in Robotics and Mechatronics Engineering at DGIST. His research interests include embedded systems, electromagnetic actuation systems, and microrobots for biomedical applications.

Hesam Khaksar is a visiting fellow at the University of Essex. He received his Ph.D. in mechanical engineering from the Iran University of Science and Technology (IUST) in 2019, and his dissertation was about dynamic modeling and control of microparticle motion behavior during 2D nanomanipulation on rough surfaces. He has been researching in the fields of medical engineering, micro/nano mechanics, soft robotics, and tribology since 2013. His visiting fellow research focuses on studying and modeling soft robotics in medical applications.

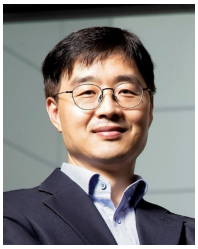

Hongsoo Choi received his M.S. (2003) and Ph.D. (2007) degrees from the School of Mechanical and Materials Engineering at Washington State University, United States. He is a Professor and Chair in the Department of Robotics and Mechatronics Engineering at Daegu-Gyeongbuk Institute of Science and Technology (DGIST). He is also the Director of the Center for Targeted Neural Networks Reconstruction of the National Science Challenge Initiatives, the Director of the first Center of Excellence, and Co-Director of DGIST-ETH Microrobotics Research Center at DGIST. He received several awards, including the Prime Minister's Commendation for Science, Information and Communication Day of Korea in 2020, the National Intellectual Property Award (Co-chairman's award) by the Presidential Council on Intellectual Property of Korea in 2019, and the Prize of the State of Geneva at the 47th International Exhibition of Inventions of Geneva, Switzerland in 2019. His research interest includes micro/nanorobotic system, neural engineering, magnetic field generating (MFG) systems, BioMEMS, piezoelectric MEMS devices, and biochip for biomedical applications.

Ali Kafash Hoshiar is a researcher in robotics and mechatronics, holding a PhD in Mechanical Engineering. Currently, he serves as an Associate Professor (Senior Lecturer) at the University of Essex, where he also leads the Robotics for Under Millimetre Intervention (RUMI) Lab. He has made several contributions to the small-scale robotics field, with notable contributions to the development of soft continuum magnetic robots, magnetic microswarms, and innovative magnetic-based mechatronic and robotics systems. His research, which is at the intersection of computational intelligence, micro/nanotechnology, and robotics, aims to develop applications in healthcare and environmental sustainability.